Heliyon 10 (2024) e30113

Contents lists available at ScienceDirect

Heliyon

journal homepage: www.cell.com/heliyon

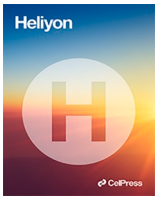

Research article

# Enhancing heat transfer efficiency in corrugated tube heat exchangers: A comprehensive approach through structural optimization and field synergy analysis

Chao Yu *, Mingzhen Shao, Wenbao Zhang, Mian Huang, Gaugnyi Wang

*Changchun Institute of Optics, Fine Mechanics and Physics, Chinese Academy of Sciences, Changchun, 130033, China*

ARTICLE INFO

*Keywords:*
Corrugated tube heat exchanger
Extreme learning machine
Nondominated sorting genetic algorithm-II
CFD

ABSTRACT

In this paper, a precise and efficient method to optimize corrugated tube heat exchangers is proposed by combining computational fluid dynamics simulation with optimization. The optimization of tubular heat exchangers involves contradictory Colburn coefficient *j*, and the friction coefficient *f*, so it is a multi-objective optimization problem. The approximate model is obtained by an extreme learning machine, and the structure parameter of the heat exchanger is optimized by the nondominated sorting genetic algorithm-II. Compared to the results between the original and optimized tube, the optimized structure Colburn coefficient increased by 5.1 % and the friction coefficient decreased by 9.3 %. Finally, the internal flow field is compared qualitatively from temperature, pressure, and velocity. The optimization effect is further emphasized by using the field synergy theory.

## 1. Introduction

As a kind of high-efficiency heat transfer surface, the corrugated tube has been used in heat exchangers. The different temperature flows through the tube respectively, a typical corrugated tube heat exchanger is shown in Fig. 1. The optimization below has resulted in high-performance heat exchangers.

Hao et al. [1] proposed three theoretical models of the plastic hinge mechanism and dynamic progressive buckling considering eccentricity and amplitude coefficients. Mozafari et al. [2] established the model of single-sided corrugated (SSC) tubes and double-sided corrugated (DSC) tubes under axial compression. The analysis showed that the total energy absorbed by DSC is significantly higher than that of SSC. Wang et al. [3] studied the heat transfer and resistance coefficients of corrugated tubes with different pitches, and evaluated the economy of the experimental system. Ashmawy et al. [4] studied the effect of surface roughness on the flow velocity and average velocity of stress-coupled fluid in sinusoidal corrugated tubes. The longitudinal and transverse corrugation on the cross-section of steel tube are studied. The results show that for longitudinal corrugations, the velocity decreases monotonously with the increase of wave number. For transverse ripple, the effect of wave number on velocity is very small. Navickaitė et al. [5] carried out numerical studies on the thermal performance of corrugated tubes under constant power conditions. The results show that the thermal efficiency of double-corrugated tubes is greatly improved under the same pressure drop. Mahbod et al. [6] introduced a new type of corrugated composite cylindrical tube to improve its impact resistance and breaking stability. The effects of corrugated shape on the crushing force efficiency and specific energy absorption of composite cylindrical tubes were studied by finite element analysis of

* Corresponding author
*E-mail address:* yuchao@ciomp.ac.cn (C. Yu).

https://doi.org/10.1016/j.heliyon.2024.e30113
Received 5 February 2024; Received in revised form 11 April 2024; Accepted 19 April 2024
Available online 25 April 2024

composite cylindrical tubes with different corrugated shapes. The results show that the compression efficiency of axial and oblique crushing can be significantly improved by the formation of a corrugated surface on the pipe. Zhang et al. [7] studied the pressure drop and heat transfer characteristics of two kinds of uniform corrugated tubes and eight kinds of non-uniform corrugated tubes, based on the finite volume method. Uhlig et al. [8] used the CFD simulation method to optimize the geometric structure of helically ribbed tubes.

Eyvazian et al. [9] carried out theoretical and experimental studies on the crushing behaviors of shallow and deep corrugation under axial loads. Sadighi et al. [10] carried out an experimental study on the exergy parameters of corrugated shell-and-tube heat exchangers. The parameters of different arrangement modes of corrugated tubes are evaluated. The results show that corrugated wear causes exergy loss and NTU increase. Sun et al. [11] show that corrugated tubes have a good synergistic effect compared with ordinary tubes. Chen et al. [12] carried out numerical and experimental studies on the heat transfer and flow characteristics of turbulent flow in asymmetric corrugated tubes. Rahim et al. [13] analyzed the crashworthiness of structural steel thin-walled corrugated tubes. Andrade et al. [14] studied the heat transfer and pressure drop characteristics of internal flow in corrugated tubes. The results show that the frictional coefficient of corrugated tubes presents a smoother transition than that of smooth tubes. It is the adiabatic and non-adiabatic frictional coefficient of corrugated tubes from laminar to turbulent flow. Corrugated tubes are more effective in transition flow. Wan et al. [15] Conducted an experimental study on the thermal performance of nanofluids flowing through the filled copper foam corrugated tubes in the heat exchange system. Wang et al. [16–19] designed new external helical corrugated tubes to achieve a balance of heat transfer, pressure drop, and energy efficiency. Reynolds stress model was also used to analyze the secondary law of turbulent flow in a new type of external helical corrugated tube. The results show that the irreversibility of heat dissipation and viscous dissipation is significantly improved by the secondary flow. Compared with transverse corrugated tubes with the same geometric parameters, spiral corrugated tubes have overall advantages. Maida et al. [20,21] use an adaptive neural fuzzy inference system to optimize shell and tube, heat exchangers. Ayush et al. [22–24] studied the effect of the expanded surface of a microchannel with variable sector angle cylindrical ribs on the heat transfer rate.

All the above researchers have made contributions to improving the performance of heat exchangers. However, further research is needed to obtain the structure size by using the optimization algorithm, within a certain size parameter range. In this research, the corrugated tube was taken as the research object, and its tube radius H, the radius of peak $R_1$, the radius of valley $R_2$, and cycle length $L$ were taken as independent variables for optimization design. The final optimization results were obtained by using the extreme learning machine (ELM) and nondominated sorting genetic algorithm-II(NSGA-II). The research provides an efficient and accurate method for heat exchanger design and fills in the method of heat exchanger optimization.

## 2. Structure parameters of corrugated tube heat exchangers

The performance and reasonable size of the heat exchanger are crucial to ensure the work of the machine. Hence, a corrugated tube is shown in Fig. 1 and the size is shown in Table .1. When the heat exchanger is working, the cold flow (water) and hot flow (pressurized air) flow through the inside and outside tube respectively.

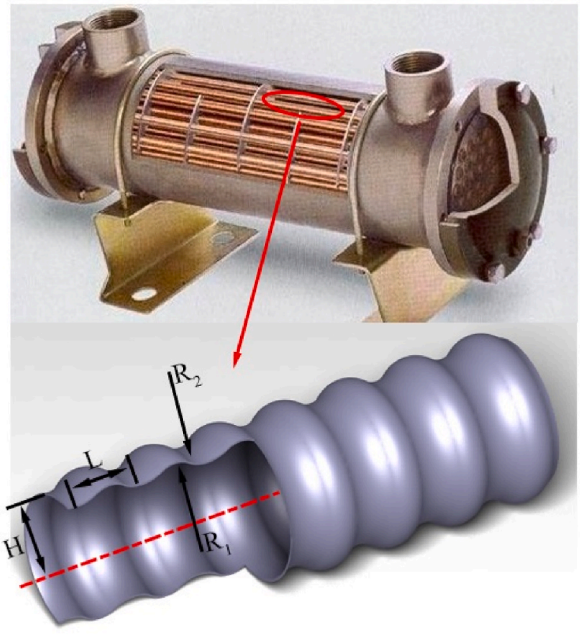


**Fig. 1.** Corrugated tube model.

## 3. Numerical simulation

### 3.1. Boundary conditions

In this research, the flow field distribution characteristics are acquired by CFD (Computational Fluid Dynamics). The standard k-ε model is chosen to solve the turbulence model [25].

Because of the uniform array of tubes in the heat exchanger, the simulation model of single channel geometry is constructed to reduce the time cost as shown in Fig. 2. The tube is surrounded by cold fluid with six prisms, and the hot fluid flows through the tube. The cold fluid flows from the outside of the bellows, and the hot fluid flows in the tube. The directions of cold and hot fluid are opposite, so the heat from the hot fluid passes through the tube to the cold fluid. In the simulation model, the hot fluid velocity is 1.5 m/s and the temperature is 411.6K as the actual working situation. At the same time, the cold fluid velocity is 1 m/s and the temperature is 313K. The outer wall of the cold fluid is set as the periodic wall.

The governing equation is solved by the finite volume method in Fluent software. The convection term and second-order upwind scheme are solved by the SIMPLE algorithm. The physical properties of fluid and solid can be found in Table 2.

The solution domain needs to be discretized, before the simulation (see Table 3). Because of the irregular structure of the corrugated tube, a tetrahedral mesh is selected for more accurate simulation result in this study by Ansys mesh, as shown in Fig. 3. The grid model should be compared to the verified grid without inertia, which the numbers of meshes are 463682, 532921, 577429, 651727, 714343, 773521 and 821566. In convective heat transfer, using Nussel as the comparison criterion, the mesh number meets the simulation requirements when the mesh increase does not affect the Nusselt result significantly, as shown in Fig. 4. Considering the calculation time and accuracy, the grid number of the simulation model is set at 714343 in this research.

### 3.2. Comparison with the experiment

CFD simulation model was constructed by referring to the experiment [11]. Fig. 5 is the comparison between CFD and experimental results. That shows good consistency with the experimental results. A series of inflow Reynolds Numbers from 10502 to 55273 is calculated to plot the pressure difference and the Nussel number, and the errors between CFD results and experimental results are less than 15 %, respectively. Therefore, the results of the simulation model are authentic.

## 4. Optimal structure of heat exchangers

Considering these two aspects, the multi-objective optimization method is employed to obtain the optimization structure in this paper. It mainly includes three parts: experimental design, approximate model establishment, and multi-objective optimization, and the specific process is shown in Fig. 6. The experimental design method of Latin hypercube sampling (LHS) was used to establish the sample points. The approximate model is constructed by ELM, and NSGA-II is adopted in this paper. The approximate model is obtained by ELM, and the structure parameter of the heat exchanger is optimized by NSGA-II. All the methods are structural optimization methods, which meet the relevant requirements of heat exchanger design and can be used as a model for bellows optimization. The approximate model is obtained by ELM, and the structure parameter of the heat exchanger is optimized by NSGA-II. All the methods are structural optimization methods, which meet the relevant requirements of heat exchanger design and can be used as a model for bellows optimization.

The purpose of optimization of corrugated tubes is to achieve high heat transfer capacity and low flow resistance of heat exchangers. The heat transfer capacity is represented by the Colburn coefficient j, and the performance of the flow resistance is represented by the friction coefficient f. The j and f can be solved by the following equation:

$$\begin{cases} j = \dfrac{Nu}{R_e P_r^{1/3}} \\ f = \dfrac{2\Delta P D}{\rho u^2 L} \end{cases} \tag{1}$$

**Table 1**
Dimensional value.

| Tube dimension | Values | Core dimensions | Values |
|---|---|---|---|
| H (mm) | 11 | Length (mm) | 954 |
| $R_1$ (mm) | 1.5 | Tube quantity | 40 |
| $R_2$ (mm) | 1.5 | Core dimension ($m^2$) | 2 |
| L (mm) | 22 | | |
| Tube thickness (mm) | 1 | | |

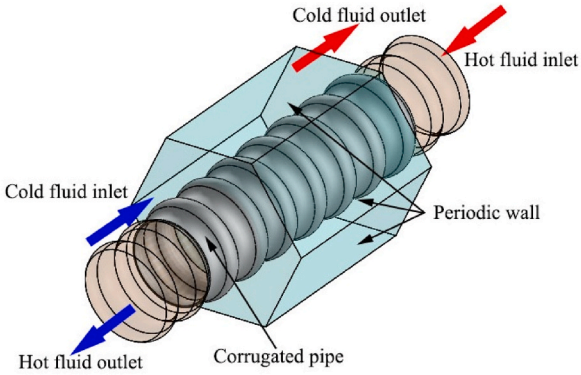


**Fig. 2.** Boundary conditions instruction.

**Table 2**
Physical properties.

| | Aluminum | Water | Air |
|---|---|---|---|
| Thermal conductivity [W/(m·K)] | 237 | 0.6 | 0.0242 |
| Specific heat [J/(kg·K)] | 871 | 4182 | 1006.43 |
| Density [kg/m$^3$] | 2719 | 998.2 | 1.23 |
| Viscosity [Pa·s] | – | $8.81 \times 10^{-4}$ | $2.493 \times 10^{-5}$ |

**Table 3**
Structural parameters change.

| | H (mm) | $R_1$ (mm) | $R_2$ (mm) | L (mm) |
|---|---|---|---|---|
| Before Optimization | 28 | 15 | 12.5 | 22 |
| After Optimization | 20 | 14.06 | 14.92 | 19.8 |

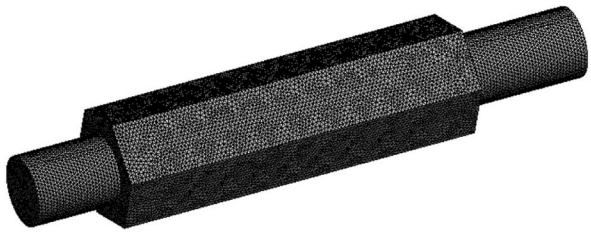

**Fig. 3.** The gird for entire computational domain.

The variable in the above equation are defined as:

$$\begin{cases} D = \dfrac{4S}{U} = \dfrac{4\pi H^2}{2\pi H} = 2H \\ Re = \dfrac{\rho D u}{\mu} \\ Pr = \dfrac{\mu c_p}{\lambda} \\ Nu = \dfrac{m c_p D(T_{out} - T_{in})}{\lambda S \Delta t_m} \end{cases} \tag{2}$$

The optimized variables are tube radius $H$, the radius of peak $R_1$, the radius of valley $R_2$, and cycle length $L$. The optimization function for the independent variable $H$, $R_1$, $R_2$, $L$ and the dependent variable $j$, $f$ can be defined as follows:

$$F(j,f) = F(H, R_1, R_2, L) \tag{3}$$

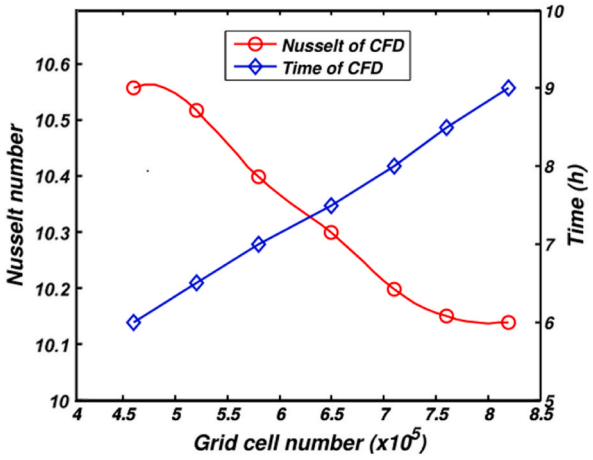


**Fig. 4.** Grid independence verification.

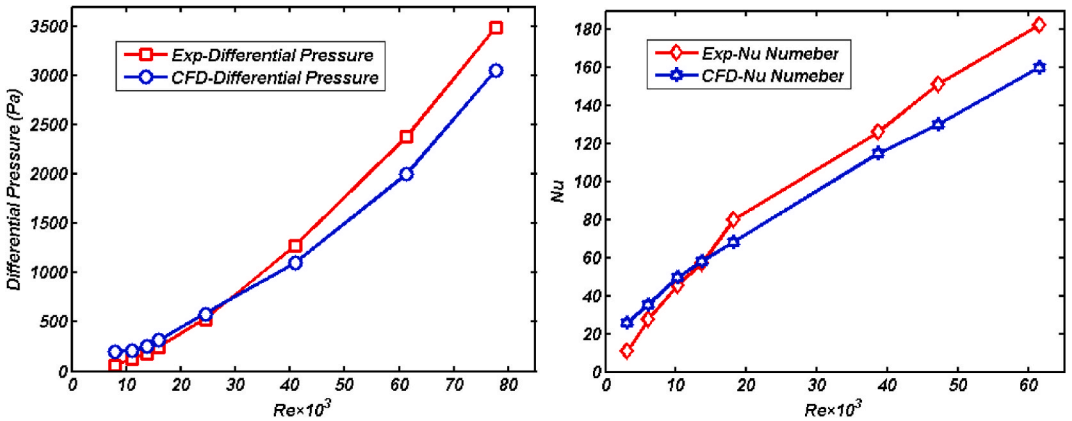


**Fig. 5.** Verification of simulation model accuracy [11].

The corrugated tube optimized variables are (mm):

$$20 < H < 40, 5 < R_1 < 15, 5 < R_2 < 15, 20 < L < 35 \tag{4}$$

With the non-linear relationship between optimized variables and optimization targets, the design of the experiment was used to assign sample points to the parameters of the tube structure by LHS in this research. The 50 groups of models were identified by LHS, listed in AppendixI. The models of each sample point are simulated. Mechanical constraints will not be taken into account during the optimization process.

The approximate model between optimization variables and optimization objectives is obtained. 20 sets of control samples were taken. Compare the errors between the approximate model and the simulation data to determine the usability of the approximate model. The root mean square error:

$$RMSE = \sqrt{\left[\sum_{i=1}^{n} (X_{CFD} - X_{\mathrm{mod}\ el})^2\right] \Big/ n} \tag{5}$$

The approximate model is available with RMSE j = 0.103, and RMSE f = 0.182. By the data of each sampling point in the approximation model, the nonlinear relationship between optimization variables and optimization objectives can be obtained, as shown in AppendixII.

The formation of vortices in the flow channel can not only improve the heat transfer ability but also increase the flow resistance. NSGA-II is chosen to get the maximum value of j/f in the approximate model, which is defined as follows.

$$\begin{aligned} &\max j(x_i) = \max F(H, R_1, R_2, L) \\ &\min f(x_i) = \min F(H, R_1, R_2, L) \end{aligned} \tag{6}$$

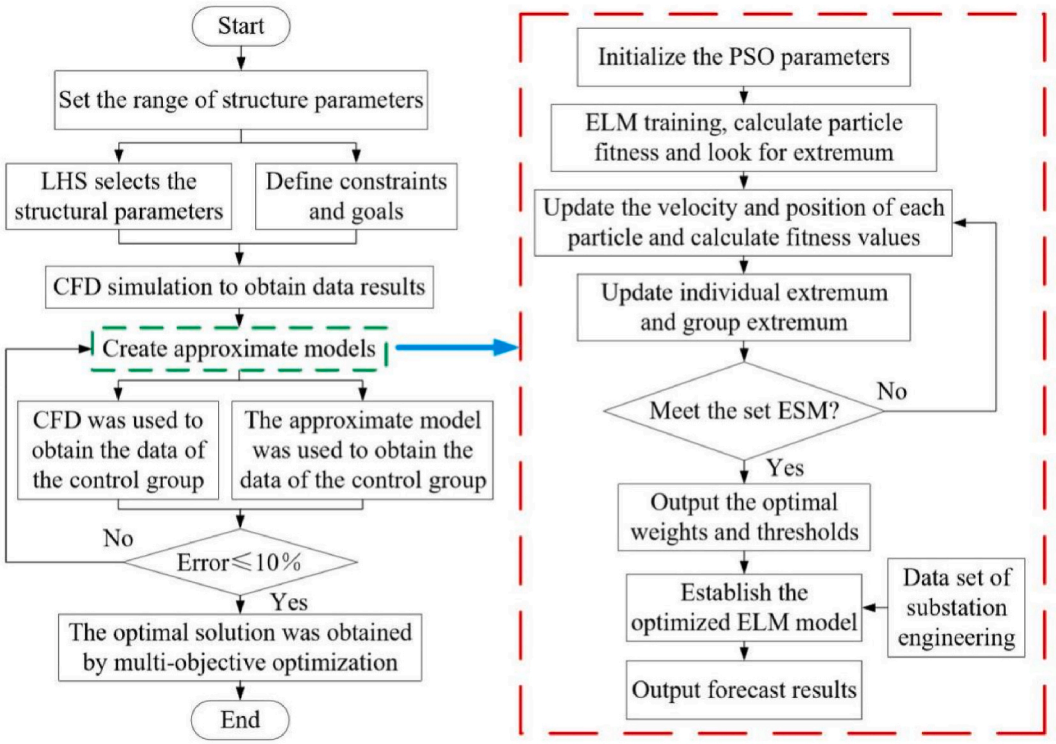


**Fig. 6.** Optimization process.

## 5. Optimal result analysis

Through the above analysis of the process of processing, the optimized corrugated tube structural parameters $H$, $R_1$, $R_2$, $L$ are obtained by the maximal $j/f$. The comparison results of the optimized structure $j$ and $f$ are obtained by approximate model, as shown in Table 4. Fig. 7 shows the changes in the structural model. The virtual model is the original model, and the entity model is the optimized model. The optimized model size is the nodule structure size under the minimum $j/f$.

Fig. 8 is the CFD cloud diagram of the tube flow field in terms of velocity, pressure and temperature before and after optimization. As the air passes through the cold wall, the pressure and the temperature gradually decrease. The optimized structure has a 10 % lower pressure difference, and the temperature difference is reduced by 7 %. For bellows heat exchangers, the smaller pressure difference means that the power of the pump can be lower. The lower temperature difference means that the heat flowing through the bellows is exchanged more fully and the heat transfer efficiency is higher.

In summary, although the diameter of the optimized corrugated tube is reduced, the frictional resistance of the fluid is reduced. The heat transfer capacity is enhanced, and the performance of the optimized corrugated heat exchanger is improved.

## 6. Discussion

### 6.1. The field synergy analysis

The corrugated tube heat exchanger in cooling process involves heat conduction and thermal convection. And the heat transfer occurs mainly in the corrugated tube border. There are two basic vector fields in this region: temperature field and velocity field. Therefore, heat transfer intensity not only depends on temperature gradient and velocity gradient, but also relates to the synergetic property of two vector fields [26]. The field synergy theory is used, which defined as follows [27–29]:

**Table 4**
Compared between the original and optimization.

| | Colburn factor $j$ | Friction factor $f$ |
|---|---|---|
| Before | 0.157 | 0.075 |
| After | 0.165 | 0.082 |
| Variation | 5.1 % | 9.3 % |

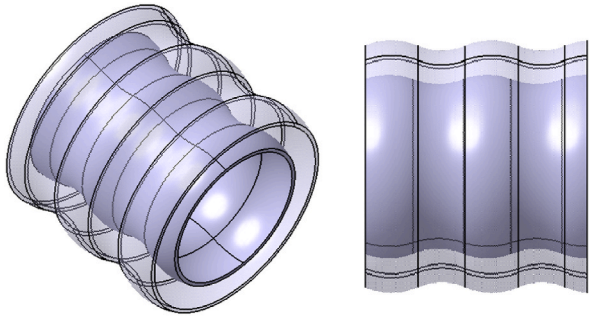

**Fig. 7.** Difference between the optimization model (entity) and the original model (virtual).

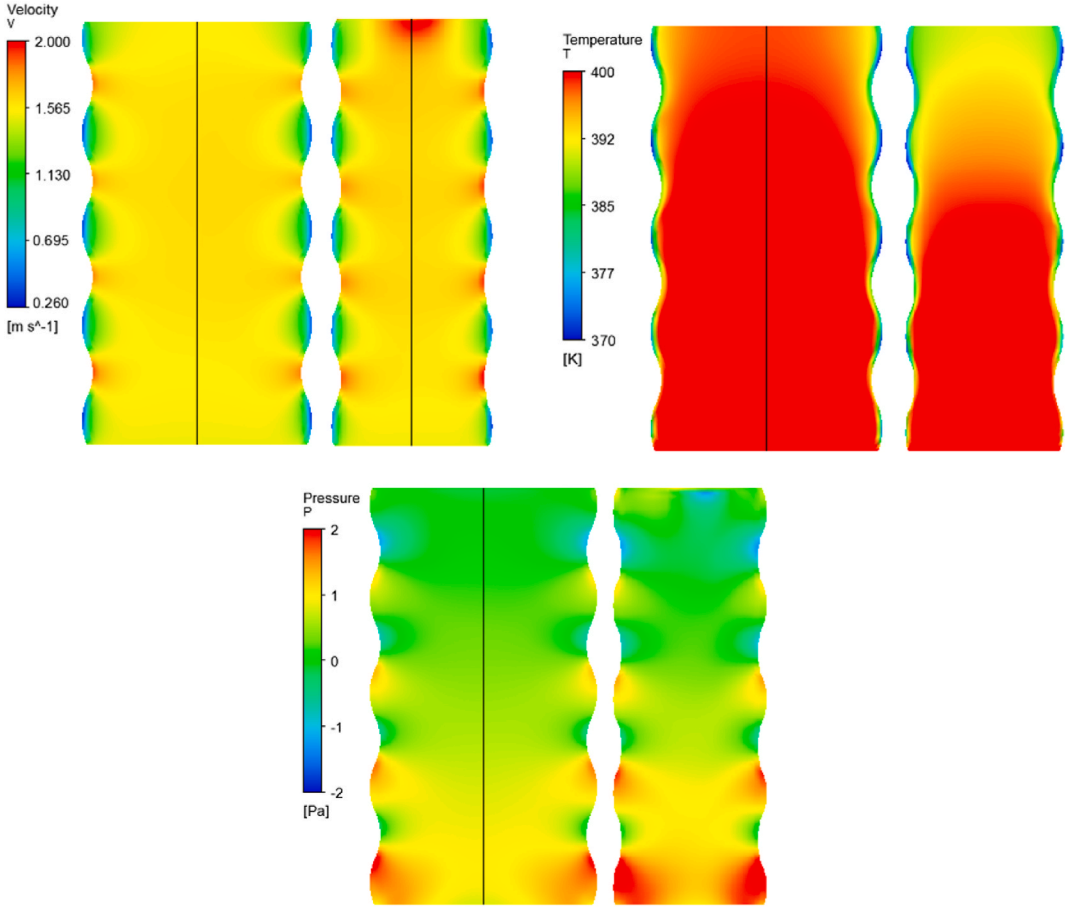


**Fig. 8.** Comparison transverse section between the optimization and the original ( left: original; right: optimization ) .

$$\begin{cases} \beta = \arccos \dfrac{U \cdot \nabla T}{|U||\nabla T|} \\ \theta = \arccos \dfrac{U \cdot \nabla p}{|U||\nabla p|} \\ \gamma = \arccos \dfrac{\nabla T \cdot \nabla u}{|\nabla T||\nabla u|} \end{cases} \tag{7}$$

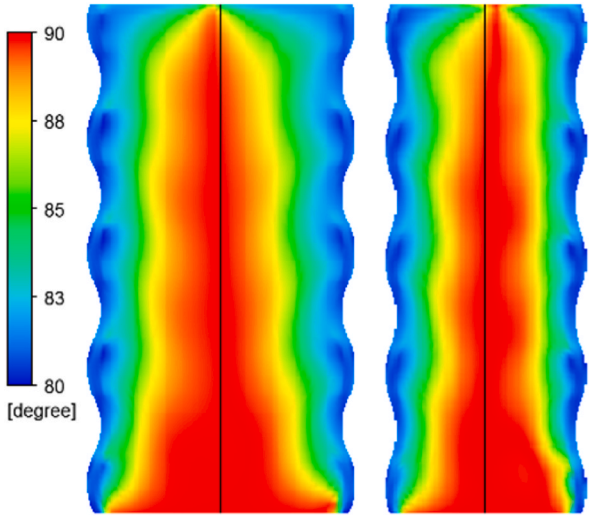


**Fig. 9.** Difference of synergy angle $\beta$

### 6.2. Synergy angle $\beta$

Fig. 9 shows the angle of the velocity and temperature gradient. According to the principle of heat transfer, air flows along the fin and the heat is transferred over the wall of the tube, at the same time. Therefore, when the velocity is perpendicular to the direction of the temperature gradient, the heat conduction enhancement effect is good. In addition, the angle is significantly reduced and the heat change is obvious at the node where the tube bends. In the middle of the tube, the temperature gradient is similar to the velocity direction, and the angle is larger. In general, the optimized model has smaller $\beta$ near the wall and in the middle of the pipeline, providing better heat transfer performance.

### 6.3. Synergy angle $\theta$

Fig. 10 shows the angle of the velocity and pressure gradient. At the bending point, the airflow is obstructed, resulting in the deviation between the flow direction and the driving force direction. As the synergy angle $\theta$ increases, the flow resistance also increases. In fact, in other places, the synergy angle of the optimized model is significantly smaller than that of the original model. It can be seen that although the pressure drop of the optimized model is relatively large, combined with the above pressure distribution. A reasonable arrangement can reduce the synergy angle, thus reducing the friction coefficient $f$.

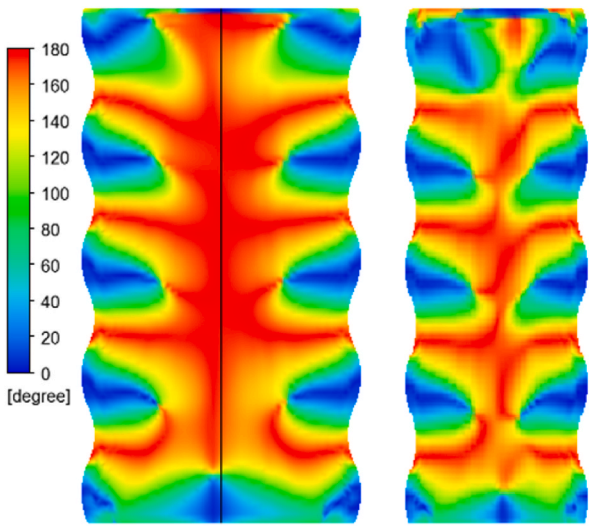


**Fig. 10.** Difference of synergy angle $\theta$

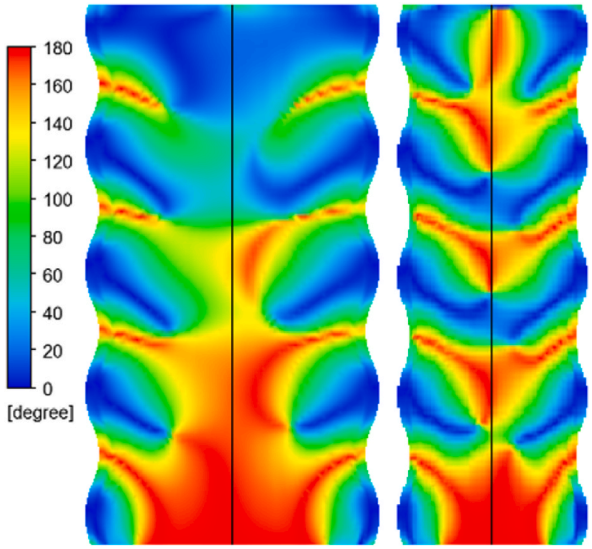


**Fig. 11.** Difference of synergy angle $\gamma$

### *6.4. Synergy angle $\gamma$*

Fig. 11 shows the synergy angle of the temperature gradient and velocity gradient. The large synergy angle $\gamma$ represents better heat transfer performance. In the process of air flowing through a corrugated tube, the fluid jets on the tube wall at the bend, forming an impingement flow field. Therefore, a large area of lower synergy angle appears at the tube bend, indicating that a more efficient heat transfer occurs here.

In summary, the optimized model has better heat transfer. The analysis of the flow field characteristics of the optimization model above is also verified better through the field synergy analysis, which better explains the rationality of the optimization method. The optimization trend can be shown more accurately through the analysis of coordination angle. The synergistic effect of the velocity field and temperature field can be considered comprehensively in heat exchanger design. The effect of the bellows heat exchanger is better when the velocity gradient and temperature gradient direction are perpendicular to each other.

## 7. Conclusion

This research selects corrugated tube heat exchangers as the object, using ELM and NSGA-II of the corrugated tube for structural optimization. After optimization, the heat exchange capability increased by 5.1 % and the flow resistance decreased by 9.3 %, thus improving the heat transfer effect. Then the internal flow field of corrugated tube is compared, and the qualitative further emphasizes the results. The optimized air temperature is reduced by 7 % and the pressure drops by 10 %. The fluid flow rate increased significantly. In general, the optimized corrugated tube heat exchangers can attain a heat transfer rate. The synergic angle is also analyzed. The optimal design method of this study can obtain a heat exchanger with better performance. The research results can provide a more efficient and accurate method for heat exchanger design. At the same time, it must be made clear that experiment is the only criterion for testing truth. The structure of the heat exchanger obtained by this optimization method still needs to be tested.

## CRediT authorship contribution statement

**Chao Yu:** Conceptualization. **Mingzhen Shao:** Data curation. **Wenbao Zhang:** Formal analysis. **Mian Huang:** Investigation. **Gaugnyi Wang:** Methodology.

## Declaration of competing interest

There is no conflict of interest in the manuscript and all authors are aware of the contribution.

## Appendix I. 50 sets of structural parameters sample points (mm)

| Code r | $L$ | $R_1$ | $R_2$ | $H$ | Code | $L$ | $R_1$ | $R_2$ | $H$ |
|---|---|---|---|---|---|---|---|---|---|
| 1 | 29.38 | 9.48 | 13.80 | 32.92 | 26 | 28.68 | 13.80 | 9.54 | 26.60 |
| 2 | 31.90 | 14.00 | 13.10 | 21.08 | 27 | 26.10 | 11.04 | 8.98 | 26.04 |
| 3 | 26.50 | 8.78 | 10.50 | 37.06 | 28 | 27.26 | 8.92 | 10.38 | 35.44 |
| 4 | 29.94 | 7.38 | 12.04 | 20.22 | 29 | 30.88 | 7.14 | 14.86 | 24.50 |
| 5 | 30.24 | 10.30 | 8.50 | 29.88 | 30 | 29.18 | 13.72 | 7.54 | 21.76 |
| 6 | 21.64 | 9.10 | 9.72 | 21.46 | 31 | 34.54 | 5.70 | 14.24 | 30.64 |
| 7 | 20.88 | 14.46 | 8.14 | 27.28 | 32 | 27.90 | 8.30 | 12.8 | 38.50 |
| 8 | 24.60 | 12.18 | 7.08 | 22.06 | 33 | 34.94 | 12.66 | 5.74 | 31.72 |
| 9 | 23.18 | 12.88 | 11.88 | 34.40 | 34 | 27.68 | 12.54 | 6.50 | 25.44 |
| 10 | 28.76 | 11.82 | 8.40 | 27.66 | 35 | 32.76 | 6.04 | 14.50 | 31.30 |
| 11 | 33.42 | 9.96 | 8.60 | 23.62 | 36 | 25.68 | 13.34 | 6.98 | 24.32 |
| 12 | 29.68 | 8.08 | 7.78 | 33.82 | 37 | 32.98 | 6.44 | 11.12 | 20.80 |
| 13 | 21.96 | 5.84 | 14.78 | 28.36 | 38 | 24.42 | 6.68 | 11.52 | 23.50 |
| 14 | 31.30 | 11.48 | 10.76 | 35.06 | 39 | 20.22 | 6.92 | 6.78 | 37.34 |
| 15 | 32.56 | 14.62 | 11.22 | 37.68 | 40 | 30.62 | 9.76 | 6.00 | 25.84 |
| 16 | 28.38 | 7.42 | 13.26 | 32.14 | 41 | 26.78 | 5.22 | 11.72 | 29.24 |
| 17 | 24.96 | 14.38 | 12.26 | 35.78 | 42 | 20.32 | 10.98 | 14.04 | 23.16 |
| 18 | 32.04 | 15.00 | 7.34 | 34.80 | 43 | 20.92 | 9.96 | 13.44 | 22.76 |
| 19 | 33.84 | 10.72 | 9.02 | 28.46 | 44 | 25.26 | 8.10 | 5.58 | 27.12 |
| 20 | 23.98 | 6.22 | 12.54 | 30.34 | 45 | 27.14 | 13.08 | 7.80 | 28.90 |
| 21 | 33.76 | 11.64 | 5.82 | 31.06 | 46 | 31.68 | 10.08 | 6.30 | 36.64 |
| 22 | 22.18 | 5.70 | 5.40 | 39.36 | 47 | 23.64 | 12.26 | 9.84 | 38.80 |
| 23 | 21.44 | 13.56 | 10.90 | 38.08 | 48 | 22.58 | 11.30 | 9.40 | 36.18 |
| 24 | 34.18 | 10.40 | 12.76 | 32.58 | 49 | 25.84 | 7.70 | 13.94 | 24.92 |
| 25 | 31.90 | 14.00 | 13.10 | 21.08 | 50 | 22.70 | 9.36 | 6.10 | 39.66 |

## Appendix II. Non-linear relationship between parameters and performances

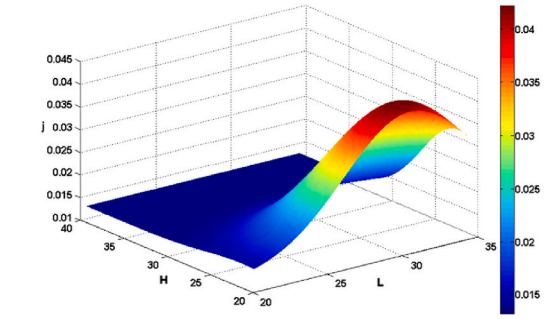


(a) $j$ *vs* $H$, $L$

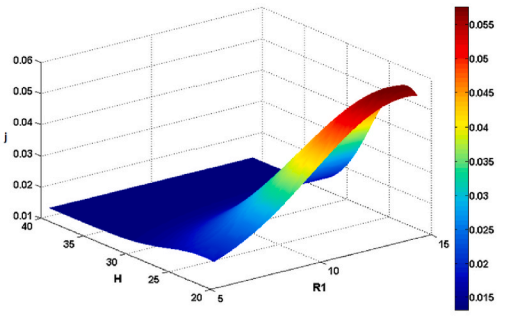


(b) $j$ *vs* $H$, $R_1$

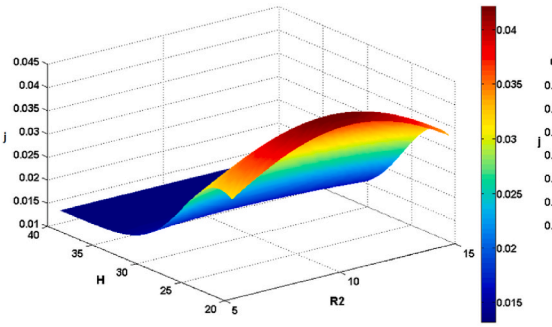


(c) $j$ *vs* $H$, $R_2$

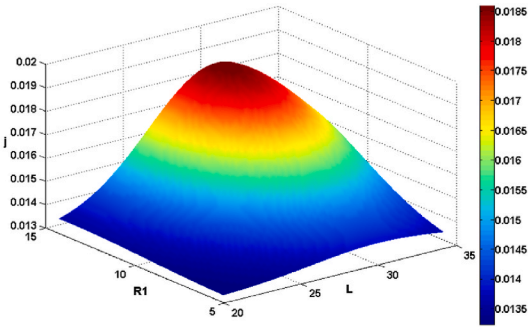


(d) $j$ *vs* $R_1$, $L$

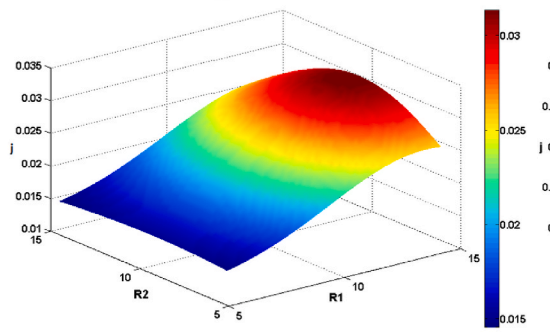


(e) $j$ *vs* $R_2$, $R_1$

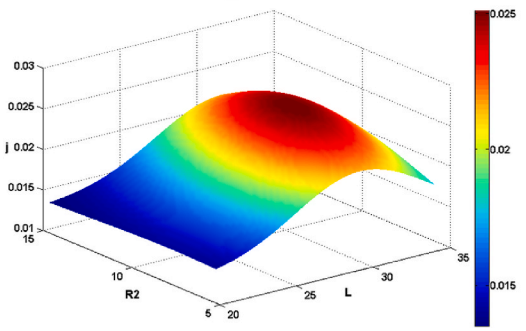


(f) $j$ *vs* $R_2$, $L$

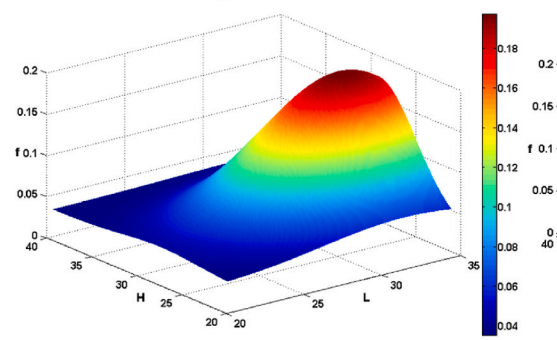


(g) $f$ *vs* $H$, $L$

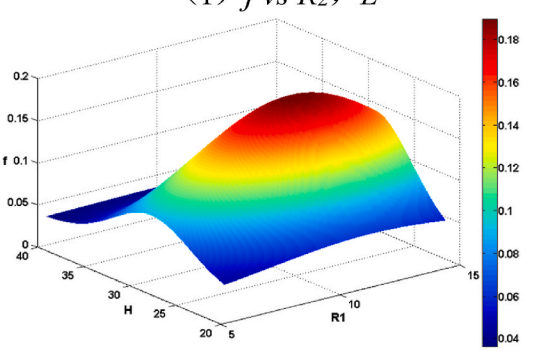


(h) $f$ *vs* $H$, $R_1$

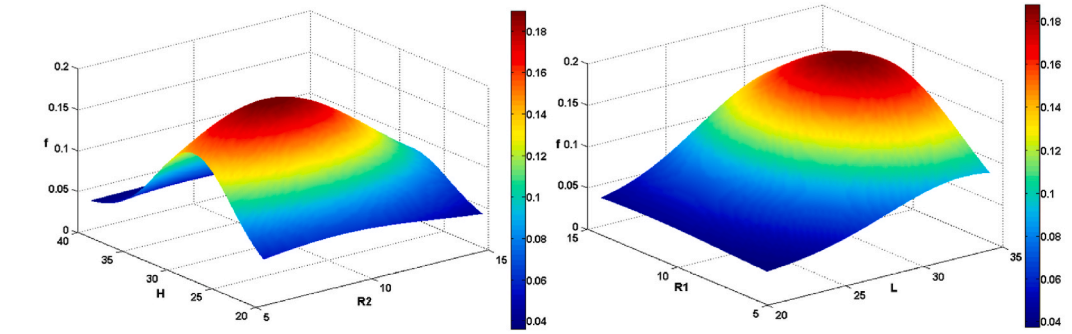


(i) $f$ vs $H$, $R_2$ (j) $f$ vs $R_1$, $L$

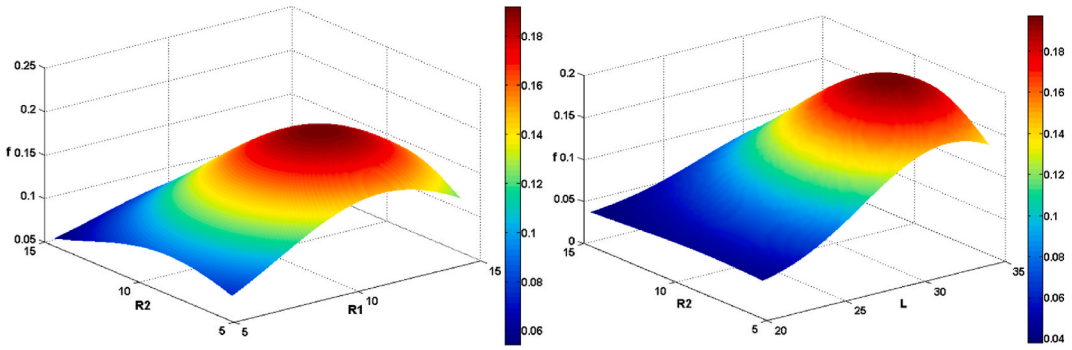


(k) $f$ vs $R_2$, $R_1$ (l) $f$ vs $R_1$, $L$

. (*continued*).

## Appendix III. 20 sets of contrast sample points (mm)

| Code r | $L$ | $R_1$ | $R_2$ | $H$ | Code | $L$ | $R_1$ | $R_2$ | $H$ |
|---|---|---|---|---|---|---|---|---|---|
| 1 | 24.24 | 12.38 | 14.08 | 22.86 | 11 | 31.02 | 12.92 | 6.72 | 30.42 |
| 2 | 21.52 | 11.62 | 10.9 | 26.62 | 12 | 20.02 | 14.12 | 9.54 | 38.04 |
| 3 | 31.88 | 7.26 | 10.16 | 20.36 | 13 | 20.96 | 8.9 | 13.12 | 37.9 |
| 4 | 28.2 | 14.84 | 12.76 | 35.52 | 14 | 22.28 | 11.12 | 6.46 | 23.94 |
| 5 | 25 | 10.44 | 7.58 | 39.4 | 15 | 32.82 | 10.96 | 8.58 | 29.5 |
| 6 | 32.56 | 13.98 | 14.8 | 34.08 | 16 | 29.62 | 9.18 | 8.42 | 24.48 |
| 7 | 30.3 | 5.78 | 5.14 | 32.24 | 17 | 26.52 | 9.6 | 11.76 | 25.34 |
| 8 | 25.54 | 5.06 | 9.32 | 28.12 | 18 | 34.48 | 6.12 | 6 | 36.9 |
| 9 | 23.5 | 8.08 | 13.84 | 33.18 | 19 | 27.46 | 6.8 | 7.04 | 31.36 |
| 10 | 33.62 | 7.62 | 11.38 | 27.24 | 20 | 28.28 | 13.24 | 12.22 | 21.12 |

## References

[1] W. Hao, J. Xie, F. Wang, Z. Liu, Z. Wang, Analytical model of thin-walled corrugated tubes with sinusoidal patterns under axial impacting, Int. J. Mech. Sci. 128–129 (2017) 1–16.
[2] H. Mozafari, S. Lin, G.C.P. Tsui, L. Gu, Controllable energy absorption of double sided corrugated tubes under axial crushing, Compos. B Eng. 134 (2018) 9–17.
[3] G. Wang, C. Qi, M. Liu, C. Li, Y. Yan, L. Liang, Effect of corrugation pitch on thermo-hydraulic performance of nanofluids in corrugated tubes of heat exchanger system based on exergy efficiency, Energy Convers. Manag. 186 (2019) 51–65.
[4] E.A. Ashmawy, Effects of surface roughness on a couple stress fluid flow through corrugated tube, Eur. J. Mech. B Fluid 76 (2019) 365–374.
[5] K. Navickaitė, L. Cattani, C.R.H. Bahl, K. Engelbrecht, Elliptical double corrugated tubes for enhanced heat transfer, Int. J. Heat Mass Tran. 128 (2019) 363–377.
[6] M. Mahbod, M. Asgari, Energy absorption analysis of a novel foam-filled corrugated composite tube under axial and oblique loadings, Thin-Walled Struct. 129 (2018) 58–73.
[7] D. Zhang, H. Tao, Y. Xu, Z. Sun, Numerical investigation on flow and heat transfer characteristics of corrugated tubes with non-uniform corrugation in turbulent flow, Chin. J. Chem. Eng. 26 (3) (2018) 437–444.
[8] R. Uhlig, B. Gobereit, J. Rheinländer, Advancing tube receiver performance by using corrugated tubes, Energy Proc. 69 (2015) 563–572.

[9] A. Eyvazian, T.N. Tran, A.M. Hamouda, Experimental and theoretical studies on axially crushed corrugated metal tubes, Int. J. Non Lin. Mech. 101 (2018) 86–94.
[10] H. Sadighi Dizaji, S. Jafarmadar, S. Asaadi, Experimental exergy analysis for shell and tube heat exchanger made of corrugated shell and corrugated tube, Exp. Therm. Fluid Sci. 81 (2017) 475–481.
[11] M. Sun, M. Zeng, Investigation on turbulent flow and heat transfer characteristics and technical economy of corrugated tube, Appl. Therm. Eng. 129 (2018) 1–11.
[12] X. Chen, H. Han, K.-S. Lee, B. Li, Y. Zhang, Turbulent heat transfer enhancement in a heat exchanger using asymmetrical outward convex corrugated tubes, Nucl. Eng. Des. 350 (2019) 78–89.
[13] M.R.U. Rahim, P.K. Bharti, A.A. Azmi, A. Umer, Axial crushing comparison of sinusoidal thin-walled corrugated tubes, Mater. Today: Proc. 5 (9, Part 3) (2018) 19431–19440.
[14] F. Andrade, A.S. Moita, A. Nikulin, A.L.N. Moreira, H. Santos, Experimental investigation on heat transfer and pressure drop of internal flow in corrugated tubes, Int. J. Heat Mass Tran. 140 (2019) 940–955.
[15] Y. Wan, R. Wu, C. Qi, G. Duan, R. Yang, Experimental study on thermo-hydraulic performances of nanofluids flowing through a corrugated tube filled with copper foam in heat exchange systems, Chin. J. Chem. Eng. 26 (12) (2018) 2431–2440.
[16] W. Wang, Y. Zhang, Y. Li, H. Han, B. Li, Multi-objective optimization of turbulent heat transfer flow in novel outward helically corrugated tubes, Appl. Therm. Eng. 138 (2018) 795–806.
[17] W. Wang, Y. Zhang, J. Liu, B. Li, B. Sundén, Numerical investigation of entropy generation of turbulent flow in a novel outward corrugated tube, Int. J. Heat Mass Tran. 126 (2018) 836–847.
[18] W. Wang, Y. Zhang, B. Li, Y. Li, Numerical investigation of tube-side fully developed turbulent flow and heat transfer in outward corrugated tubes, Int. J. Heat Mass Tran. 116 (2018) 115–126.
[19] W. Wang, Y. Zhang, K.-S. Lee, B. Li, Optimal design of a double pipe heat exchanger based on the outward helically corrugated tube, Int. J. Heat Mass Tran. 135 (2019) 706–716.
[20] R. Reyes, B.M.R. Maida, L. Jorge, O.F. De, H. Cristiano, Thermo ecological optimization of shell and tube heat exchangers using NSGA II, Appl. Therm. Eng.: Design, processes, equipment, economics (2019) 156.
[21] B.R.R. Maida, L.M.R. Jorge, H.F. Cristiano, Determination of design and operation parameters of a surface condenser using an adaptive neuro-fuzzy inference system, Int. J. Heat Mass Tran. 138 (2019) 17–24.
[22] N. Kumari, T. Alam, M.A. Ali, A.S. Yadav, N.K. Gupta, M.I.H. Siddiqui, D. Dobrotă, I.M. Rotaru, A.A. Sharma, Numerical investigation on hydrothermal performance of micro channel heat sink with periodic spatial modification on sidewalls, Micromachines 13 (2022) 1986.
[23] A.P. Dash, T. Alam, M.I.H. Siddiqui, P. Blecich, M. Kumar, N.K. Gupta, M.A. Ali, A.S. Yadav, Impact on heat transfer rate due to an extended surface on the passage of microchannel using cylindrical ribs with varying sector angle, Energies 15 (2022) 8191.
[24] S. Saha, T. Alam, M.I.H. Siddiqui, M. Kumar, M.A. Ali, N.K. Gupta, D. Dobrotă, Analysis of microchannel heat sink of silicon material with right triangular groove on sidewall of passage, Materials 15 (2022) 7020.
[25] S.J. Kline, F.A. McClintock, Describing uncertainties in single-sampleexperiments, Mech. Eng. 75 (7) (1953) 3–9.
[26] W.M. Kays, A.L. London, Compact Heat Exchangers, 1984.
[27] Z.Y. Guo, W.Q. Tao, R.K. Shah, The field synergy (coordination) principle and its applications in enhancing single phase convective heat transfer, Int. J. Heat Mass Tran. 48 (9) (2005) 1797–1807.
[28] W. Liu, Z.C. Liu, S.Y. Huang, Physical quantity synergy in the field of turbulent heat transfer and its analysis for heat transfer enhancement, Sci. Bull. 55 (23) (2010) 2589–2597.
[29] C. Yu, X. Xue, K. Shi, M. Shao, A three-dimensional numerical and multi-objective optimal design of wavy plate-fins heat exchangers, Processes 9 (1) (2021) 9.